VERSÃO SUBMETIDA – **SUBMITTED VERSION**
Please use the following link to access the published version: https://doi.org/10.1016/j.ceramint.2020.08.210

INFLUENCE OF THE FORMING METHOD ON FLASH SINTERING OF ZnO CERAMICS

Ana Gabriela Storion[1]*, Julieta Adriana Ferreira[1], Eliria M. J. A. Pallone[1] - *anagstorion@usp.br

[1]University of São Paulo, 225 Duque de Caxias Norte Ave, Pirassununga, SP 13635-900, Brazil

ABSTRACT

This work aimed to investigate different forming techniques used in the ceramic industry when applied to flash sintering. It was studied how the density gradient interferes with the final densification and microstructural heterogeneity development of ZnO specimens. For this purpose, ZnO cylindrical specimens were formed by uniaxial pressing, isostatic pressing, and slip casting. All experiments were conducted isothermally at 800 °C in an adapted tube furnace, with an applied electric field of 60 V/cm and 200 mA/mm^2 as maximum current density. Samples formed by isostatic pressing showed better control in the development of the microstructural homogeneity. The ones formed by slip casting had the lower apparent density and longer incubation time among all forming methods. Also, slip casting formed samples showed the largest detachment of the average grain size in the central region compared to the other regions, among all the forming methods. One outstanding result is related to differences between the regions close to the upper and lower electrodes in the samples formed by uniaxial pressing, even if using alternating current mode. These results showed that density distribution along the green specimen should be considered a decisive factor when evaluating samples flash sintered. The chosen forming technique causes significant differences both in the incubation time, densification, and in the development of microstructural heterogeneity.

Key Words: ZnO, Flash Sintering, Forming, Density Gradient.

1. Introduction

Flash Sintering was firstly reported by Cologna et al in 2010 [1] and has been successfully applied to the consolidation of several materials since then [2–5]. Some studies have shown that energy consumption in flash sintering is highly reduced when compared to conventional sintering [6,7]. However, for industrial-scale application, besides the optimization of energy consumption during sintering, homogeneous microstructural development must be evaluated to avoid compromising the required properties. Different forming methods result in different density gradients which consequently lead to heterogeneity in the distribution of the powder throughout the part, which influences the sintering step [8,9].

Among the most commonly used industrial forming methods are the compaction processes from dry powder (such as uniaxial or isostatic) and shape casting from a dispersion of a ceramic powder (such as slip casting) [10–12]. Dry powder compaction generates density gradients throughout the part as a result of combining the induced external compaction pressure, the friction between the material and the die-wall, as well as the inter-particle friction [13]. In the isostatic pressing, the difference in the actuation of the loads inside the specimen is minimized, since the pressure is transmitted to the part through the pressurized fluid in a practically equal manner in all directions [8].

Liquid forming processes are based on colloidal systems, in which loads promoted by the removal of the liquid are used for the consolidation of suspended particles [11]. In the slip casting process, the liquid is removed by a pressure gradient as it flows through a porous mould [12,14]. In general, mechanical compaction is the most widely used forming

technique in the ceramic manufacturing industry; however, the variation of the applied stress along the material can generate high density gradients, which compromise the properties of the final product. Although pressure variations are minimized when using isostatic pressing, the technique presents a higher cost [14]. Yet, isostatic pressing provides less control in handling green body properties than shape casting forming methods [8,9,11,13].

The microstructural heterogeneity of a flash sintered material has been widely discussed in the literature and is still a barrier to applying this technique on a larger scale [15–17]. This heterogeneity can be a function of several factors, such as the formation of thermal gradients along with the specimen; differences in the electrochemical reduction potentials in the regions near the electrodes; creation of hotspots, among others [14,18]. Carvalho et al (2018) [19] and Muccillo et al (2017) [20] studied the influence of material porosity prior to flash sintering on the final microstructure. The authors state that the distribution of pores plays a fundamental role in the formation of electric current paths.

Therefore, this work aims to explore the different forming methods used in the ceramic industry in which flash sintering can be applied and to understand the influence of these methods on the microstructural development of ZnO. It is also important to evaluate how the pore distribution and the density gradient interfere in its densification and microstructural heterogeneity when submitted to flash sintering.

2. Experimental Procedure

Samples were prepared using 99% ZnO commercial powder (Synth®), and the average particle size was determined by laser diffraction (Horiba - LA-950V2). Three forming techniques were used in the forming of specimens

with 6 mm diameter and 5 mm height: uniaxial pressing, isostatic pressing, and slip casting.

For the dry powder compaction, a mixture of the ZnO powder and 0,5% 4-aminobenzoic acid (PABA, Vetec LTDA) by mass was ball milled in an alcoholic medium for 6 h. After that period 0,5% oleic acid (Vetec LTDA) by mass was added to the suspension and mixed for 2 h. The resulting suspension was dried under continuous air flow until the alcohol was eliminated and then passed through an 80-mesh sieve. The samples were uniaxially pressed under two different loads, 140 and 300 MPa, and isostatically pressed under 200 MPa (AIP CP360). For the slip casting, the suspension was prepared with a powder-to-water weight ratio of 2:1, with the addition of 1 % of ammonium polyacrylate by mass, and ball milled for 12 h. The suspension was then poured into a porous plaster cast. The specimens were then calcined at 500 °C for 1 h at a heating rate of 2 °C min^{-1}.

Since each forming method has different green densities, dilatometry test was performed to analyze the behavior of the ZnO in a conventional furnace and to establish a temperature for performing the flash sintering tests. For comparison purposes, conventional sintering at 1200 °C for 120 min was performed at a heating rate of 5 °C min^{-1} for isostatically shaped specimens. Both sintering (conventional and flash) were performed in the same tubular furnace adapted to perform the flash sintering in order to reduce experimental differences [15] under an applied mechanical pressure of 300 kPa.

For the flash sintering experiments the following parameters were used: maximum electrical current density of 200 mA/mm^2 and electrical field of 60 V/cm in AC mode (alternating current); frequency of 1000 Hz (sine waveform). No conductive pastes were used in the contact between the samples and the Pt electrode. The electrical source was switched on

after a 5 min furnace step at 800 °C, and the flash sintering experiments occurred isothermally with a steady-state of 60 s (after the current density reached its maximum value).

The apparent density of the specimens was determined based on the Archimedes principle (ASTM C373-88, 2006) and the values were described in terms of theoretical density. Microstructural characterization of the fracture surface was performed using scanning electron microscopy (SEM - Philips - FEG XL30 equipment). The fractured surface was analyzed in four different regions: near the upper and lower electrodes, core and radial surface, according to Figure 1. ImageJ software was used to calculate the grain size distribution in each region [21]. The Tukey test was performed with a significance level of 5%, assuming equality between the grain sizes means. It was considered for the analyses of two images for each region with a count of 100 grains each.

Figure 1 – Fracture section of the specimen in the radial center, indicating the regions in which the micrographs were obtained, being two regions close to the upper and lower electrodes, one in the central region (core) and the other in the radial surface.

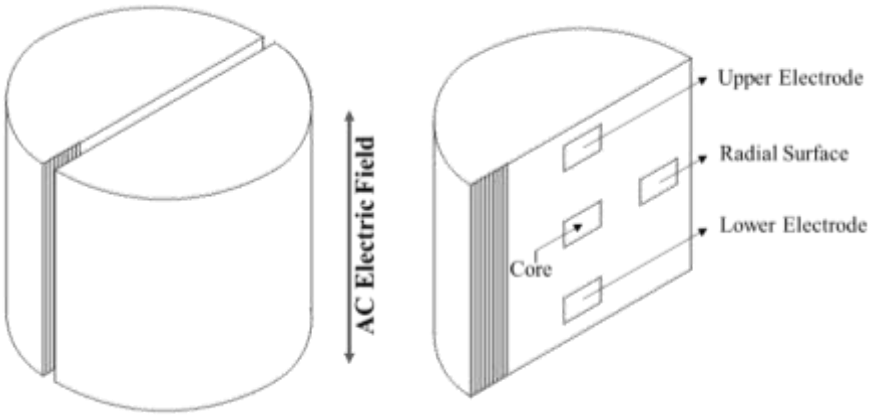

3. Results and Discussion

According to the laser diffraction, the ZnO powder has dimensions of 70 ± 30 nm. Figure 2 shows the curve obtained from the dilatometric test. It is noted that no change occurs up to approximately 600 °C and the material has a maximum densification rate of approximately 800 °C. According to the graph, the temperature of 800 °C was chosen to perform a 5 min step before applying the electrical voltage in the flash sintering experiments. This step was performed to avoid differences concerning the green density caused by the forming methods.

Figure 2 – Dilatometry test for ZnO, plotting the linear shrinkage curve, relative density and densification rate as a function of temperature.

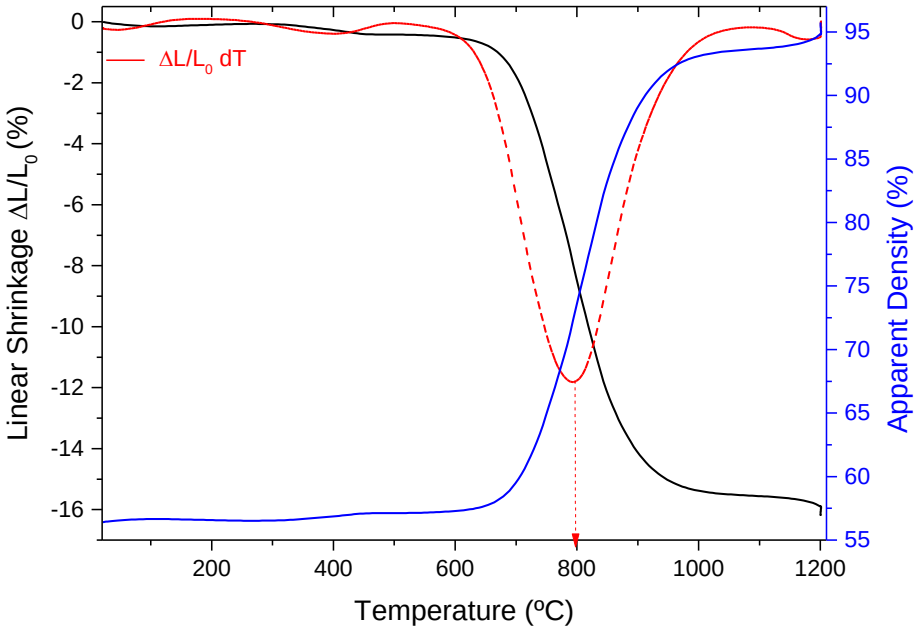

Table 1 describes the incubation time (s) and apparent density (%TD) of the specimens according to the different forming methods and sintering conditions. A deviation from the apparent density averages is observed for specimens formed by slip casting. When comparing only the samples

formed by uniaxial pressing, a load increase from 140 to 300 MPa caused a higher dispersion of the values. Since the pressure gradient generated inside the specimen is dependent on the applied load [22], it could explain these differences. Larger loads generate higher stress distribution heterogeneity, and may also exceed the maximum packaging load supported by particles in some regions.

The variation in pore distribution according to the forming method directly affects the particle-part contact, which can lead to different electric current paths in an uneven way [20,23]. This may generate thermal gradients along the part, causing regions of uneven densification, which can affect the final density [15,16].

The slip casting method showed the lowest apparent density values and the longest incubation times. This fact shows that the forming method, and consequently the green density gradient, influences the electrical resistivity of the specimen, significantly modifying the incubation time. Some studies related to the densification rate of materials during flash sintering take into account the green density and the instantaneous density of the material, assuming them to be homogeneous throughout the entire specimen [24–26]. However, the results shown in this paper show that the distribution of particle packing interferes with both the onset of flash sintering and the densification of the specimen. This factor can be significant in determining the flash event, in addition to the critical combinations between furnace temperature and the electrical parameters used.

Figure 3 and Table 2 present, respectively, the micrographs obtained by SEM of the fracture surface in the different regions and the average grain sizes of the specimens formed by different methods and sintered under different conditions. It can be seen for all regions analyzed that the grain size was smaller using flash sintering when compared to

conventional sintering, as previously demonstrated in the literature [1,26]. The suppression of grain growth in flash sintering can take place through the association of several factors [27]: electric field interactions with grain boundaries [28], the high heating rate provided by the Joule effect [23,29], the rate at which the process occurs [18,20], among others [30,31].

Table 1 – Incubation time (s) and Apparent Density (%TD) of the specimens formed by different methods and conventionally and flash sintered.

Forming	Sintering	Incubation time (s)	Apparent Density (%TD)
Isostatic Press	Conventional	-	94,5 ± 0,8
Isostatic Press	Flash	151 ± 50	94,3 ± 0,3
Uniaxial Press (140 MPa)	Flash	166 ± 30	94,7 ± 1,4
Uniaxial Press (300 MPa)	Flash	173 ± 18	93,1 ± 2,3
Slip Casting	Flash	457 ± 7	91,4 ± 0,2

Table 2 – Average grain size (µm) of specimens formed by different forming methods and conventionally and flash sintered.

	Upper Electrode	Lower Electrode	Core	Radial Surface
Conventional	12,63±2,27^{a}	13,64±1,59^{a}	14,08±2,33^{a}	12,79±2,38^{a}
Isostatic (FS)	2,03±0,67^{a}	2,22±0,73^{a}	3,43±1,06^{b}	2,51±0,69^{c}
Uniaxial 140 (FS)	1,92±0,59^{a}	1,15±0,58^{b}	4,03±1,15^{c}	2,43±1,10^{a}
Uniaxial 300 (FS)	2,09±0,65^{a}	1,57±0,50^{b}	3,15±0,94^{c}	2,58±0,83^{d}
Slip Casting (FS)	0,81±0,24^{a}	0,93±0,23^{a}	2,27±0,58^{b}	0,77±0,18^{a}

^{a,b,c,d} equal letters indicate that the results do not differ significantly according to Tukey's test. The results compare the different regions to each other within the same forming method, but do not compare the different forming methods to each other.

Figure 3 - Micrography obtained by SEM for the analyzed regions of the specimens formed by different methods and conventionally and flash sintered.

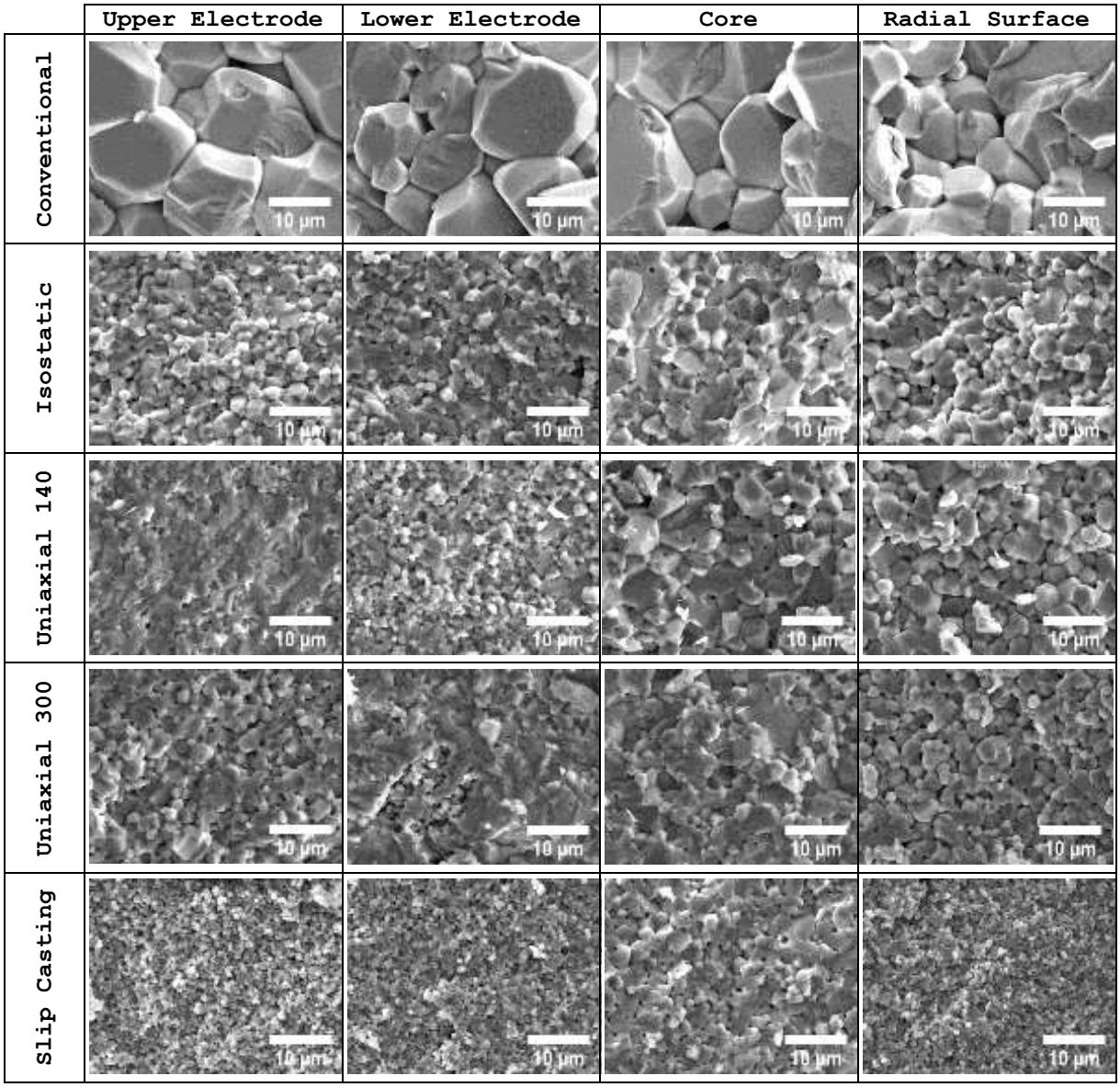

Figure 4 shows the Tukey test results for grain sizes for the different regions according to the forming methods and conditions studied. According to Figures 3 and 4, the central region tends to present grains with larger dimensions than the others. This behavior can be explained by the fact that at high temperatures (which the specimen reaches by the Joule effect), there is heat loss by radiation and convection from the specimen to the environment (at a lower temperature) [16,22,32][32]. This

loss occurs most dramatically over the surface of the specimen. This causes a heat flow towards the center outwards, generating a thermal gradient along with the specimen. As the interior remains at a higher temperature than the outer surface, and for a longer period of time, grain growth is induced in this region. This behavior is typical of cylindrical specimens [4,16,33,34].

Another characteristic can be noticed in flash sintered samples, in which the regions corresponding to the proximity of the electrodes present smaller dimensions than the others. This fact may be associated with the contact of these regions with the electrodes, which are made of thermally conductive material. This causes more severe heat loss than in other regions due to the contribution of conduction loss (in addition to heat loss from convection and radiation), creating a lower temperature zone [15,16,31,32]. Furthermore, Liu et al. (2018) reported a temperature gradient along with the specimen during the steady-state of flash sintering. The regions near the electrodes were under lower temperatures than the other regions. The authors suggested that this could be associated with heat release during oxidation and reduction reactions that occur at the ends of cathode-electrolyte-anode contact. They also state that the formation of defects in the regions near the contacts, which are usually endothermic (consuming energy from the vicinity), may be responsible for the lower temperature.

VERSÃO SUBMETIDA – **SUBMITTED VERSION**
Please use the following link to access the published version: https://doi.org/10.1016/j.ceramint.2020.08.210

Figure 4 –Tukey's mean difference with 5% significance for grain size in conventional sintering and flash sintering of specimens formed by slip casting, isostatic pressing at 200 MPa (isostatic), uniaxial pressing at 140 MPa (UP140) and uniaxial pressing at 300 MPa (UP300).

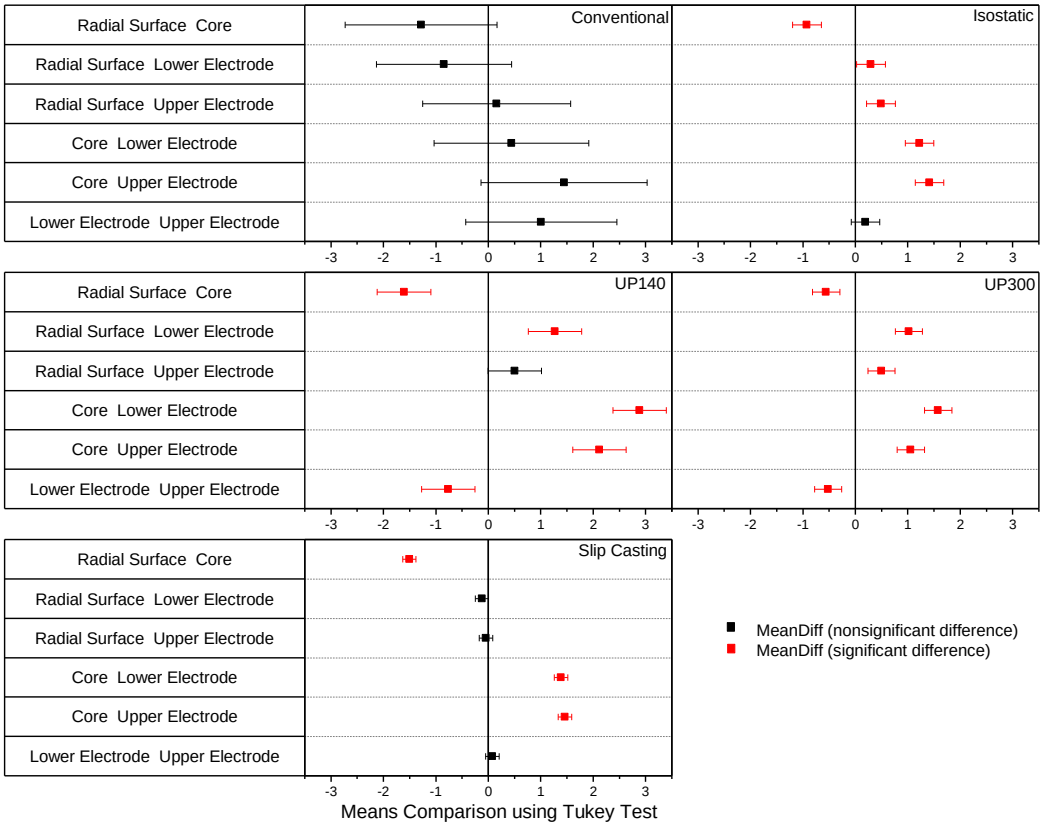

In the microstructural analysis presented in Figure 3, the conventionally sintered specimens showed similarities in the grain size distribution in the different regions analyzed. The specimens isostatically formed and flash sintered showed similar mean grain size between the upper and lower electrodes, but different grain sizes between the radial surface and the central region. Although statistically different, the average grain size on the radial surface is closer to the electrode regions than to the central region. This supports the fact that the thermal gradient generated along with the specimens, due to heat losses, occurs more intensively in the electrode's regions (where

conduction takes place) than on the radial surface. In addition, both regions remain at a lower temperature than the core.

The uniaxially formed samples presented higher differences between the most external regions in relation to the central region. There was a statistical similarity of the average grain sizes between the radial surface and the upper electrode, with the other regions showing significant differences. For the uniaxial pressing at 300 MPa, the same pattern is observed, and the region of the upper electrode showed an increased grain growth when compared to the lower electrode.

Although all the regions presented significant differences, in this case, there is again a tendency to approximate the values of the upper electrode region with the radial surface region. This fact may be associated with the density gradient formed during the uniaxial pressing since the applied load occurred in a single axis (longitudinal axis). This causes particle-particle contact to be favored on one side of the punch and near the extreme regions of the radial surface along the cylinder [13]. This fact corroborates the influence of the density gradients generated in green compaction.

Some authors have shown that the application of direct current (DC) in flash sintering has revealed significant differences in grain sizes near the positive and negative electrode regions [26,33,35–37]. However, the use of alternating current (AC), as employed in this study, presented the same microstructural differences. This suggests that the contribution of the density gradient during green compaction is significant in the evolution of the microstructure, in addition to the electrodes reactions [35,38,39].

For the slip casting method, all regions showed statistical similarity except for the central region. When compared to other forming methods, especially concerning isostatic pressing (due to the better

dispersion of the loads along the specimen), a suppressed grain growth is noticed. Nevertheless, the final density of the slip casting specimens was lower. Although colloidal suspension methods present greater control of powder dispersion, the lower charge applied on contact between particles may require more intense electrical conditions during densification.

Figure 5 shows the behavior of electric field curves, electric current density and power density for the different forming methods. After sintering, the electric field stabilized at: 32.9 V/cm for the isostatic pressing, 34 V/cm for the uniaxial pressing at 140 MPa, 38.2 V/cm for the uniaxial pressing at 300 MPa, and 38.6 V/cm for the slip casting. Although the specimens were subject to the same electrical current density, the different density distributions along the specimen influence the electrical resistivity of the material. As previously mentioned, these differences are caused by how contact between the particles is established in the green compact. These gradients do not influence in a significant way conventional sintering. However, during flash sintering, current density and Joule heating are strongly influenced by the geometry of the particles as well as the contact area between them [40,41]. Unequal packaging may generate localized heating and impact the consolidation of the material, as verified in this study.

Figure 5 - Current Density (J), Electric Field (E), and Power Density (P) flash sintering curves for the specimens formed by isostatic pressing, uniaxial pressing at 140 MPa (UP140), uniaxial pressing at 300 MPa (UP300) and slip casting.

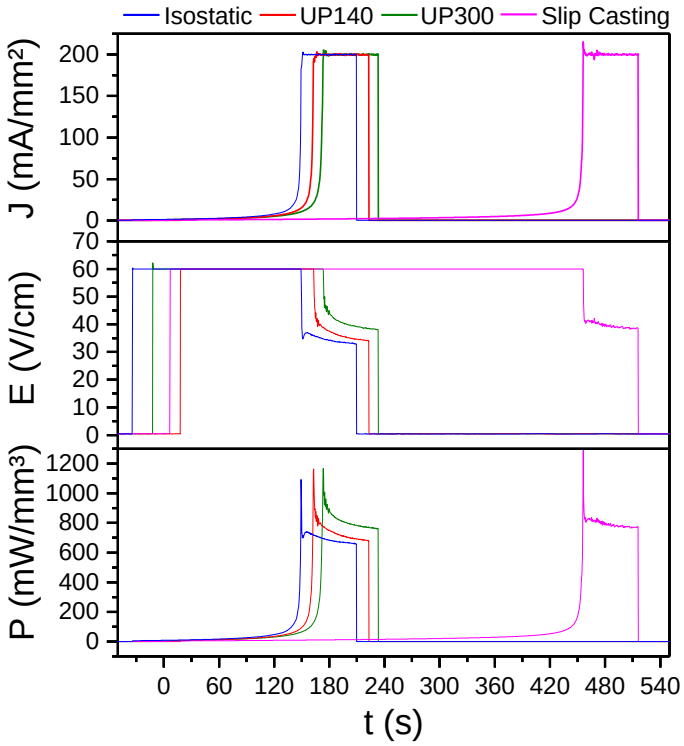

Figure 6 summarizes the behavior of the microstructural distribution of the specimens formed by the different forming methods, followed by their relative densities. This figure emphasizes the dispersion of the grain size of each region around the total average value. When considering flash sintering, the only forming method in which all regions converged with the average value was isostatic pressing. This fact supports the previous discussions that this method improved microstructural development control. Regarding slip casting, it can be observed the similarity between the regions except the central region, which substantially diverged from the others. Regarding the uniaxial presses, both showed large dispersion around the average with all regions, confirming a lower microstructural control provided by this method. The

results presented in Figure 6 reinforce the influence of forming methods on the microstructural development of specimens flash sintered. In this context, the isostatic pressing method showed the best results concerning densification coupled with better microstructural homogeneity along the specimen.

Figure 6 – Average grain size for each region and apparent density for conventional and flash sintering of specimens formed by isostatic pressing at 200 MPa (isostatic), slip casting, uniaxial pressing at 140 MPa (UP140) and uniaxial pressing at 300 MPa (UP300).

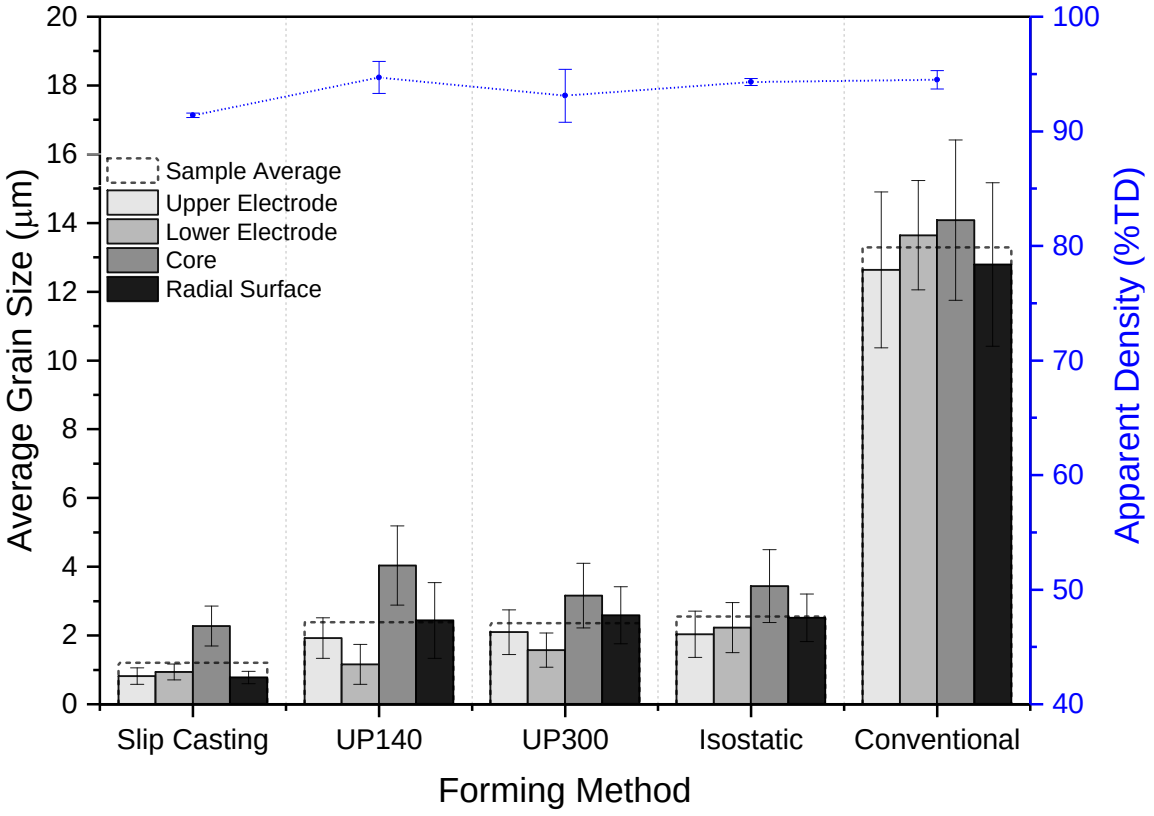

Conclusions

The different forming techniques resulted in microstructural and densification differences. Isostatic pressing and slip casting forming methods showed microstructural differences between the central region and

the others (more pronounced). However, the regions near the lower and upper electrodes showed microstructural similarities between each other. The uniaxial pressing, regardless of the applied load, presented a difference between the regions near to the lower and upper electrodes, despite the use of AC. This strengthens the influence of the load distribution applied along the green specimen on microstructural development during flash sintering. Isostatic pressing provided greater control in microstructural homogeneity among all the methods used. The results indicate that the green density distribution generated in the forming stage should be considered a decisive factor when evaluating specimens submitted to flash sintering. The choice of the forming method will lead to significant differences in both incubation time, relative density, and microstructural heterogeneity.

Acknowledgements

The authors thank the São Paulo Research Foundation (FAPESP) for its funding, processes number 2015/07319-8 and 2018/11143-0, and the Coordenação de Aperfeiçoamento de Pessoal de Nível Superior - Brazil (CAPES) – finance code 001.

References

[1] M. Cologna, B. Rashkova, R. Raj, Flash Sintering of Nanograin Zirconia in <5 s at 850°C, J. Am. Ceram. Soc. 93 (2010) 3556–3559. https://doi.org/10.1111/j.1551-2916.2010.04089.x.

[2] H. Bicer, B. Beyoglu, T.E. Ozdemir, J. Okasinski, T. Tsakalakos, Direct in situ observation of electric field assisted densification of ZnO by energy dispersive X-ray diffraction, Ceram. Int. 45 (2019) 7614–7618. https://doi.org/10.1016/j.ceramint.2019.01.057.

[3] C.A. Grimley, A.L.G. Prette, E.C. Dickey, Effect of boundary conditions on reduction during early stage flash sintering of YSZ, Acta Mater. 174 (2019) 271–278. https://doi.org/10.1016/j.actamat.2019.05.001.

[4] E. Taghaddos, H. Charalambous, T. Tsakalakos, A. Safari, Electromechanical properties of flash sintered BNT-based piezoelectric ceramic, J. Eur. Ceram. Soc. 39 (2019) 2882–2888. https://doi.org/10.1016/j.jeurceramsoc.2019.03.050.

[5] X.L. Phuah, H. Wang, H. Charalambous, S.K. Jha, T. Tsakalakos, X. Zhang, H. Wang, Comparison of the grain growth behavior and defect structures of flash sintered ZnO with and without controlled current ramp, Scr. Mater. 162 (2019) 251–255. https://doi.org/10.1016/j.scriptamat.2018.11.009.

[6] C.L. Ojaimi, J.A. Ferreira, A.L. Chinelatto, A.S.A. Chinelatto, E.M. de J.A. Pallone, Microstructural analysis of ZrO2/Al2O3 composite: Flash and conventional sintering, Ceram. Int. 46 (2020) 2473–2480. https://doi.org/10.1016/j.ceramint.2019.09.241.

[7] D. Heidary, M. Lanagan, C.A. Randall, Contrasting energy efficiency in various ceramic sintering processes, J. Eur. Ceram. Soc. 38 (2018) 1018–1029. https://doi.org/10.1016/j.jeurceramsoc.2017.10.015.

[8] L.F. Francis, Powder Processes, in: Mater. Process., Elsevier, Online, 2016: pp. 343–414. https://doi.org/10.1016/B978-0-12-385132-1.00005-7.

[9] L.S.A. Schiavo, P.Q. Mantas, A.M. Segadães, R.C.D. Cruz, From dry pressing to plastic forming of ceramics: Assessing the workability window, Constr. Build. Mater. 189 (2018) 594–600. https://doi.org/10.1016/j.conbuildmat.2018.09.015.

[10] L. DEJONGHE, M. RAHAMAN, 4.1 Sintering of Ceramics, in: Handb. Adv. Ceram., Elsevier, Online, 2003: pp. 187–264.

https://doi.org/10.1016/B978-012654640-8/50006-7.

[11] M. Rahaman, Ceramic processing and sintering, 2ª, CRC Press, Boca Raton, 2003.

[12] J.S. Reed, Principles of Ceramics Processing, 2ª ed, John Wiley & Sons, New York, 1995.

[13] J. Fruhstorfer, C.G. Aneziris, Influence of particle size distributions on the density and density gradients in uniaxial compacts, Ceram. Int. 43 (2017) 13175–13184. https://doi.org/10.1016/j.ceramint.2017.07.011.

[14] C.B. Carter, M.G. Norton, Ceramic Materials - Science and Engineering, Springer US, New York, 2007.

[15] J.V. Campos, I.R. Lavagnini, R.V. de Sousa, J.A. Ferreira, E.M. de J.A. Pallone, Development of an instrumented and automated flash sintering setup for enhanced process monitoring and parameter control, J. Eur. Ceram. Soc. 39 (2019) 531–538. https://doi.org/10.1016/j.jeurceramsoc.2018.09.002.

[16] I. R. Lavagnini, J.V. Campos, J.A. Ferreira, E.M.J. A. Pallone, Microstructural evolution of 3YSZ flash-sintered with current ramp control, J. Am. Ceram. Soc. (2020) jace.17037. https://doi.org/10.1111/jace.17037.

[17] C. Cao, R. Mücke, O. Guillon, Effect of AC field on uniaxial viscosity and sintering stress of ceria, Acta Mater. 182 (2020) 77–86. https://doi.org/10.1016/j.actamat.2019.10.035.

[18] T.A. Ring, Ceramic Green Body Formation, in: Fundam. Ceram. Powder Process. Synth., Elsevier, Online, 1996: pp. 609–679. https://doi.org/10.1016/B978-012588930-8/50017-6.

[19] S. Carvalho, E. Muccillo, R. Muccillo, Electrical Behavior and Microstructural Features of Electric Field-Assisted and Conventionally Sintered 3 mol% Yttria-Stabilized Zirconia, Ceramics.

1 (2018) 3–12. https://doi.org/10.3390/ceramics1010002.

[20] E.N.S. Muccillo, S.G.M. Carvalho, R. Muccillo, Electric field-assisted pressureless sintering of zirconia–scandia–ceria solid electrolytes, J. Mater. Sci. 53 (2018) 1658–1671. https://doi.org/10.1007/s10853-017-1615-3.

[21] U. S. National Institutes of Health, Image Processing and Analysis in Java., Available in Https://Imagej.Nih.Gov/Ij/. (2020).

[22] H.A. Al-Qureshi, A. Galiotto, A.N. Klein, On the mechanics of cold die compaction for powder metallurgy, J. Mater. Process. Technol. 166 (2005) 135–143. https://doi.org/10.1016/j.jmatprotec.2004.08.009.

[23] S. Carvalho, E. Muccillo, R. Muccillo, Electrical Behavior and Microstructural Features of Electric Field-Assisted and Conventionally Sintered 3 mol% Yttria-Stabilized Zirconia, Ceramics. 1 (2018) 3–12. https://doi.org/10.3390/ceramics1010002.

[24] J.G.P. Silva, H.A. Al-Qureshi, F. Keil, R. Janssen, A dynamic bifurcation criterion for thermal runaway during the flash sintering of ceramics, J. Eur. Ceram. Soc. 36 (2016) 1261–1267. https://doi.org/10.1016/j.jeurceramsoc.2015.11.048.

[25] R.I. Todd, E. Zapata-Solvas, R.S. Bonilla, T. Sneddon, P.R. Wilshaw, Electrical characteristics of flash sintering: thermal runaway of Joule heating, J. Eur. Ceram. Soc. 35 (2015) 1865–1877. https://doi.org/10.1016/j.jeurceramsoc.2014.12.022.

[26] A. Eqbal, K.S. Arya, T. Chakrabarti, In-depth study of the evolving thermal runaway and thermal gradient in the dog bone sample during flash sintering using finite element analysis, Ceram. Int. (2020) 0–1. https://doi.org/10.1016/j.ceramint.2020.01.034.

[27] J. Luo, The scientific questions and technological opportunities of flash sintering: From a case study of ZnO to other ceramics, Scr.

Mater. 146 (2018) 260–266. https://doi.org/10.1016/j.scriptamat.2017.12.006.

[28] S. Ghosh, A.H. Chokshi, P. Lee, R. Raj, A Huge Effect of Weak dc Electrical Fields on Grain Growth in Zirconia, J. Am. Ceram. Soc. 92 (2009) 1856–1859. https://doi.org/10.1111/j.1551-2916.2009.03102.x.

[29] M. Biesuz, V.M. Sglavo, Flash sintering of ceramics, J. Eur. Ceram. Soc. 39 (2019) 115–143. https://doi.org/10.1016/j.jeurceramsoc.2018.08.048.

[30] R. Chaim, Y. Amouyal, Liquid-film assisted mechanism of reactive flash sintering in oxide systems, Materials (Basel). 12 (2019) 1–9. https://doi.org/10.3390/ma12091494.

[31] O. Guillon, J. Gonzalez-Julian, B. Dargatz, T. Kessel, G. Schierning, J. Räthel, M. Herrmann, Field-assisted sintering technology/spark plasma sintering: Mechanisms, materials, and technology developments, Adv. Eng. Mater. 16 (2014) 830–849. https://doi.org/10.1002/adem.201300409.

[32] Y. Zhang, J. Nie, J.M. Chan, J. Luo, Probing the densification mechanisms during flash sintering of ZnO, Acta Mater. 125 (2017) 465–475. https://doi.org/10.1016/j.actamat.2016.12.015.

[33] K. Terauds, J.-M. Lebrun, H.-H. Lee, T.-Y. Jeon, S.-H. Lee, J.H. Je, R. Raj, Electroluminescence and the measurement of temperature during Stage III of flash sintering experiments, J. Eur. Ceram. Soc. 35 (2015) 3195–3199. https://doi.org/10.1016/j.jeurceramsoc.2015.03.040.

[34] Y. Dong, I.W. Chen, Electrical and hydrogen reduction enhances kinetics in doped zirconia and ceria: II. Mapping electrode polarization and vacancy condensation in YSZ, J. Am. Ceram. Soc. 101 (2018) 1058–1073. https://doi.org/10.1111/jace.15274.

[35] G. Liu, D. Liu, J. Liu, Y. Gao, Y. Wang, Asymmetric temperature distribution during steady stage of flash sintering dense zirconia, J. Eur. Ceram. Soc. 38 (2018) 2893–2896. https://doi.org/10.1016/j.jeurceramsoc.2018.02.012.

[36] Y. Zhang, J. Jung, J. Luo, Thermal runaway, flash sintering and asymmetrical microstructural development of ZnO and ZnO–Bi2O3 under direct currents, Acta Mater. 94 (2015) 87–100. https://doi.org/10.1016/j.actamat.2015.04.018.

[37] H. Charalambous, S.K. Jha, K.H. Christian, R.T. Lay, T. Tsakalakos, Flash Sintering using Controlled Current Ramp, J. Eur. Ceram. Soc. 38 (2018) 3689–3693. https://doi.org/10.1016/j.jeurceramsoc.2018.04.003.

[38] W. Qin, H. Majidi, J. Yun, K. van Benthem, Electrode Effects on Microstructure Formation During FLASH Sintering of Yttrium-Stabilized Zirconia, J. Am. Ceram. Soc. 99 (2016) 2253–2259. https://doi.org/10.1111/jace.14234.

[39] M. Biesuz, L. Pinter, T. Saunders, M. Reece, J. Binner, V. Sglavo, S. Grasso, Investigation of Electrochemical, Optical and Thermal Effects during Flash Sintering of 8YSZ, Materials (Basel). 11 (2018) 1214. https://doi.org/10.3390/ma11071214.

[40] R. Serrazina, P.M. Vilarinho, A.M.O.R. Senos, L. Pereira, I.M. Reaney, J.S. Dean, Modelling the particle contact influence on the Joule heating and temperature distribution during FLASH sintering, J. Eur. Ceram. Soc. 40 (2020) 1205–1211. https://doi.org/10.1016/j.jeurceramsoc.2019.12.015.

[41] R. Serrazina, J.S. Dean, I.M. Reaney, L. Pereira, P.M. Vilarinho, A.M.O.R. Senos, Mechanism of densification in low-temperature FLASH sintered lead free potassium sodium niobate (KNN) piezoelectrics, J. Mater. Chem. C. 7 (2019) 14334–14341.